Eco-friendly Hybrid Paper–AgBr–TiO_2 for efficient Photocatalytic aerobic Mineralization of Ethanol

Mouheb Sboui[a,b*], Marina Cortés-Reyes[a]*, Meenakshisundaram Swaminathan[c], Luis J. Alemany[a]

[a]Departamento de Ingeniería Química, Facultad de Ciencias, Campus de Teatinos, Universidad de Málaga, Málaga E-29071, Spain

[b]University of Sfax, Faculty of Sciences, BP1171-3018 Sfax, Tunisia

[c]Nanomaterials Laboratory, International Research Centre, Kalasalingam Academy of Research and Education, Krishnankoil- 626126, India

*Corresponding authors:

E-mail addresses: marinacr@uma.es (M. Cortés-Reyes), sboui.mouheb@gmail.com (M. Sboui)

Abstract

In this study, a facile and effective route to prepare hybrid photocatalysts (paper–TiO_2, paper–TiO_2–AgBr and paper–AgBr–TiO_2) has been reported. The preparation procedure consisted of the direct adsorption of the previously synthesized titania nanoparticles (TiO_2 sol) to generate the TiO_2 nanosphere and the immersion process in an aqueous suspension of AgBr to form the AgBr nanoclusters on paper fibers. The synthesis technology is economic, efficient, environmentally friendly and easy to implement even at industrial scale. A cellulose-based structure with well dispersed TiO_2 particles of around 1 μm and a pseudo-liquid coating of Ag^+ and AgBr species was obtained. All the prepared photocatalysts demonstrated effective photocatalytic performance in gaseous phase ethanol degradation with simulated sunlight illumination, through the direct mineralization to CO_2 and the parallel reaction via acetaldehyde degradation. A relevant improvement in the photocatalytic activity was noticed when TiO_2 was associated with AgBr nanocrystals, with a higher effect observed when AgBr was loaded onto the paper surface prior to TiO_2. Ag–Ti interaction reduces the pair recombination rate and increases the available charge carriers generating reactive OH- radicals from both Ag-species and TiO_2, and O_2^- radicals from Ag^+–AgBr species, which would be involved in the ethanol degradation process.

Keywords: Paper-AgBr-TiO_2; ethanol photodegradation; surface functionalization; sunlight irradiation

1. Introduction

Semiconductor photocatalysis is being presented as a suitable solution for environmental and energy problems (Bian et al., 2014; Jiménez-Tototzintle et al., 2018; Liu et al., 2015; Sboui et al., 2017; W.-S. Wang et al., 2013; Zhang et al., 2015). Among the semiconductor photocatalysts, titanium dioxide (TiO_2) has been considered as one of the most suitable used material as a result of its high performance, nontoxicity, good chemical inertness, long–term stability, inexpensive and ecological friendly character (Qian et al., 2019; S.-H. Wang et al., 2013).

Nevertheless, the use of TiO_2 to reduce environmental pollutants is still limited and below expectations. One of the disadvantages is the separation and reuse of the titania in powder form when it is used in slurry, as well as the precipitation in the solution and the tendency of the particles to aggregate, which control the possibility of using TiO_2 nanoparticles in photocatalysis applications. Furthermore, the photocatalytic activity of TiO_2 is essentially limited to UV domain due to its wide band gap (3.0–3.2 eV) and the rapid recombination rate of each hole-electron (h^+/e^-) pair (Xu et al., 2020).

TiO_2 coating on a flexible support is an excellent approach to recover the catalyst and reuse it. Among the different substrates reported in the literature, paper–TiO_2 nanostructures have received special attention because of the incorporation of the characteristics of TiO_2 and cellulose paper into a high-performance material. The main advantages of cellulose papers are their low cost, high availability, flexibility, lightness, environmentally friendly character, well thermal stabilization up to 250 °C, bending capacity and good mechanical properties (Abdel Rehim et al., 2016; Pelton et al., 2006). Moreover, the specific structure of cellulose that contains a high number of surface hydroxyl groups favors the bond between TiO_2 and cellulosic fibers by cellulose–O–Ti bridging (Daoud and Xin, 2004). This structure provides a good

template for the generation of TiO_2. Therefore, the cellulose paper substrate presents a series of properties that make it more attractive in comparison with traditional rigid substrates.

The first description of the use of papermaking technique to produce paper–TiO_2, obtaining active materials in the degradation with air of acetaldehyde under weak fluorescent light, was performed by (Matsubara et al., 1995). Since then, several papers focused on the improvement of the immobilization approach and the enhancement of the photocatalytic activity of the hybrid paper–TiO_2 in the removal of several pollutants, such as volatile organic compounds (VOCs), dyes or amines, have been reported. It is noteworthy that the origin of these toxic compound emission, such as ethanol, is anthropogenic and their control is crucial (Carbuloni et al., 2020; Ferrero et al., 2018) being their photodegradation an efficient solution (Hitam and Jalil, 2020).

The methodology of immobilization and incorporation and the uses of materials obtained by the functionalization of paper with metal oxide nanostructures, as TiO_2, are still under review (Chauhan et al., 2015; Pelton et al., 2006). Currently, two methods are used to incorporate photocatalyst to the paper during its synthesis process. The first method is known as the wet-end addition, where TiO_2 is mixed with the paper mill suspension and this mixture is filtered during the paper formation. Nevertheless, through this method, only a small portion of TiO_2 particles can be embedded within the paper and, in addition, there is the possibility of aggregation between these particles during the process of embedding, which would limit the photocatalytic performance. The second method is the coating of TiO_2 on the paper by the impregnation of the dry paper with the TiO_2 suspension by passing a two-roll press. In this process, the presence of a binder is often necessary to link TiO_2 NPs with the paper, which can negatively affect the photocatalytic performance of TiO_2. Therefore, the development of a more effective method is necessary to immobilize TiO_2 nanoparticles on paper in a controlled manner without compromising the flexibility of the paper and its thermal or chemical stability. One

method is the direct adsorption of the previously synthesized titania nanoparticles (TiO_2 sol) onto the paper followed by a mild drying process to enhance the irreversible anchoring of the TiO_2 NPs on the fiber surface. The advantages of this technique are its easy implementation and the certainty of the obtaining of an effective fiber coating with uniform particles of TiO_2. However, the shift to the visible light range cannot be reached by the immobilization of TiO_2 on the cellulose paper. For that, the association of TiO_2 with a semiconductor that shows a narrower band gap, such as AgBr (E_g =2.6 eV), might be the alternative to improve the photocatalytic activity in the visible region through a more effective separation of photogenerated electrons and holes and, in addition, it can also prevent the recombination (Cui et al., 2018; Wang et al., 2012).

Despite the strong interest of researchers in the field of photocatalysis in recent years, especially its applications in the environmental field, it remains below expectations, especially when it comes to systematic studies that explain the effect of photocatalytic paper association with another catalyst and the extent of the impact of this association on the photocatalytic properties of hybrid paper–TiO_2 and the consequently improvement in pollutant reduction. Therefore, this paper is focused on the study of the association of AgBr with paper–TiO_2, depending on the order of preparation, and its influence on the mineralization of ethanol, as a model VOC, under simulated sunlight illumination at room temperature.

2. Materials and methods

2.1. Materials

The chemical compounds (provided by Aldrich) employed in this study were titanium butoxide ($Ti(OBu)_4$ ≥97%), silver nitrate ($AgNO_3$≥99.8%), potassium bromide (KBr≥99%), isopropyl alcohol (C_3H_7OH ≥99.5%), nitric acid (HNO_3≥ 65%) and ethanol (C_2H_5OH ≥99.0%). All of

them were of analytical grade. The cellulose source (paper) used was a filter paper supported by Whatman.

2.2. Synthesis of photocatalysts

TiO_2 sol solution was prepared adding slowly 1.5 (w/v) % solution of $Ti(OBu)_4$ to 30 mL of isopropyl alcohol under constant stirring until it became gel. After that, the sample was dried at 80 °C in oven for 3 h and then, 20 mL of HNO_3 (1 M) was added drop by drop to the mixture under continuous stirring at room temperature. Afterwards, it was introduced in an autoclave and heated at 130 °C for 3 h to produce TiO_2 sol nanoparticles. Once TiO_2 sol solution was cooled to room temperature, the immersion of a pure cellulose paper in this solution was carried out for 4 h. After removing the paper from the TiO_2 sol solution, the sample was dried at 60 °C for 3 h, and this sample was named as paper–TiO_2.

On the other hand, paper–AgBr–TiO_2 was prepared by immersing a pure cellulose paper in 20 mL of AgBr solution (10^{-3} M) for 4 h at room temperature. Then, the sample was thoroughly washed with water and dried at 60 °C for 3 h. Subsequently, the paper–AgBr was immersed into TiO_2 sol for 4h at room temperature and, finally it was dried at 60 °C for 3 h. A series of catalysts was prepared using this procedure and changing the concentration of AgBr solution between 10^{-5} and 10^{-1} M.

To analyze the influence of the incorporation order to the catalyst, paper–TiO_2–AgBr, was also prepared using the same synthesis steps as in the preparation of paper–AgBr–TiO_2 but using paper–TiO_2 instead of pure cellulose paper. To summarize, the preparation methods employed in this work for the synthesis of paper–TiO_2, paper–TiO_2–AgBr and paper–AgBr–TiO_2 are displayed in Figure 1.

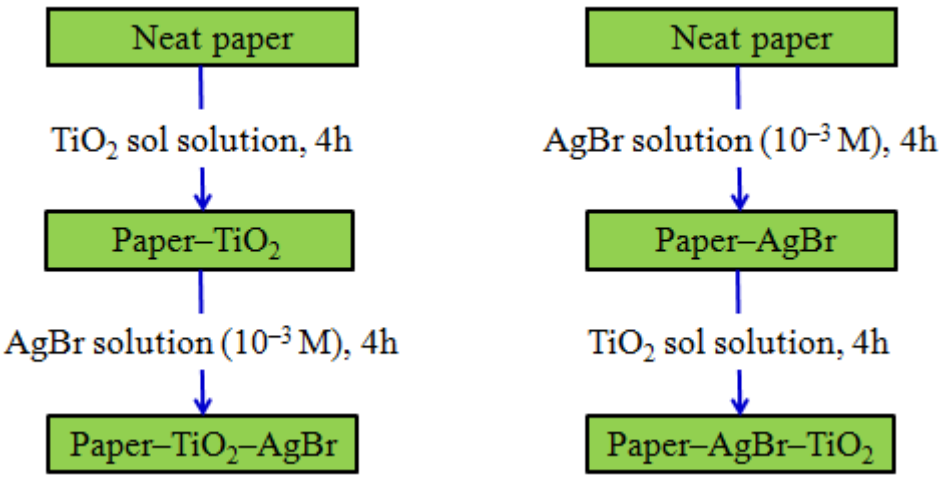

Figure 1. Scheme of the procedure followed in the hybrid photocatalyst preparation.

2.3. Characterization of photocatalysts

The synthesized materials were analyzed using several techniques in order to study their physical and chemical properties. Raman spectroscopy was used to analyze the crystalline phase of each sample, using a LabRAM Analytical Raman micro-spectrograph, with a He-Ne laser source (λ=632.8 nm) and CCD detector. The surface morphology of hybrid photocatalysts was studied by scanning electron microscopy (SEM) obtained with the JEOL JSM-840 microscope. The chemical composition of hybrid photocatalysts has been studied by X-ray photoelectron spectroscopy (XPS) with a PHI Versa Probe II spectrometer, which works with unmonochromatized Al Kα source (1486.7 eV) at 14 kV and 15 mA. The regions of Ti2p, O1s, Ag3d and Br3d were analyzed and the carbon C1s peak centered at 284.8eV was used as internal standard to determine peak positions within ±0.2 eV accuracy. The optical properties of the materials were studied at room temperature by UV–vis diffuses reflectance spectrophotometer (DRS, TU-1901), and Photoluminescence (PL) spectroscopy (Fluorolog 3–21, Horiba Jobin Yvon, France). X-ray diffraction (XRD) patterns were registered using a BRUKER AXS diffractometer (Bruker AXS, Madison, WI) with a Cu-Kα radiation, generated at 30 kV, and an

incident current of 100 mA. Samples consisting of a thin film of the photocatalysts were analyzed from 10° to 65° (2θ), using scanning steps of 0.05º and 100 s per step. In order to quantify the silver content, ICP measurements were carried out over the samples after the digestion of the paper and using an inductively coupled plasma atomic emission spectrometer (ICP-AES Perkin-Elmer OPTIMA 3000).

2.4. Photoactivity experiments

To verify the efficiency and ability of the photocatalysts that were prepared in this study to remove ethanol in gas phase, a series of photodegradation experiments of ethanol was conducted in a cylindrical batch-type reactor of Pyrex glass (height: 14.0 cm, diameter: 9.0 cm and volume of 890 cm^3). The photocatalytic paper was placed in the reactor as a 7 cm diameter circle.

Before starting the experiments, the reactor was purged of any gas by cleaning it with oxygen for 1 h. Thereafter, ethanol was injected by a septum located inside wall of the photoreactor. The initial concentration of ethanol in gas phase was stabilized at 100 µM.

The reactor ~~is~~ was placed in the center of the SOLARBOX apparatus which has a Xenon lamp (500 W) simulating solar energy and placed at the top. It also contains a water filter located between the reactor and the lamp to keep the heat of reactor at room temperature. Before starting the irradiation process with the Xenon lamp, the apparatus was maintained in the dark for 1 h in order to balance the adsorption between the catalyst and the pollutant (ethanol). The duration of one test for each catalyst took 5 h of illumination and 200 µL of gas was periodically taken from the reactor via a gas–tight syringe for analysis. GC–17A Shimadzu gas chromatograph with a HP–1 column and a flame ionization detector (FID) was used to monitor the concentration of ethanol and the intermediate products, whereas CO_2 content was quantified by an HP6890 gas chromatograph with a 60/80 Carboxen column and a TCD.

The percentage of ethanol conversion in the reactor is expressed by the following equation (eq. 1):

$$\text{Conversion (\%)} = \frac{[\text{ethanol}]_{\text{in}} - [\text{ethanol}]_{\text{out}}}{[\text{ethanol}]_{\text{in}}} \cdot 100 \quad (1)$$

where $[\text{ethanol}]_{in}$ and $[\text{ethanol}]_{out}$ are the molar concentrations at the inlet and outlet of ethanol, respectively.

The percentage of conversion to CO_2 was calculated using the following equation:

$$\text{Mineralization (\%)} = \text{Conversion to } CO_2(\%) = \frac{[CO_2]_{out}}{n \cdot [\text{ethanol}]_{\text{in}}} \cdot 100 \quad (2)$$

where $[CO_2]_{out}$ represents the concentration of CO_2 measured at the outlet of the photocatalytic reactor and n represents the number of carbon atoms that ethanol contains.

In addition, the photocatalytic stability of the samples was analyzed with recycling experiments. For that, four cycles of illumination with a duration of 120 min were carried out, with an intermediate process between them that consisted of keeping the sample in the oven at 70 ºC during 30 minutes and then 1 hour in the reactor under oxygen atmosphere in order to reactivate the catalyst.

3. Results and discussion

3.1. Characterization of materials

Raman spectroscopy is a powerful and rapid technology to identify TiO_2, even when is associated with other material in a low amount. In Figure 2, the spectra for both untreated and treated paper by TiO_2 as well as AgBr are shown to verify the structure of each sample. The spectrum for neat paper (a) is similar to that previously reported (Liu et al., 1998; Sboui et al., 2018) and corresponds to the typical bands of cellulose I, with characteristic modes around 400, 1100 and 1400 cm^{-1} related to the cellulosic ring deformation, the β-1,4- glycosidic linkages of the D-glucose units and H-C-H and H-O-C bending modes of cellulose.

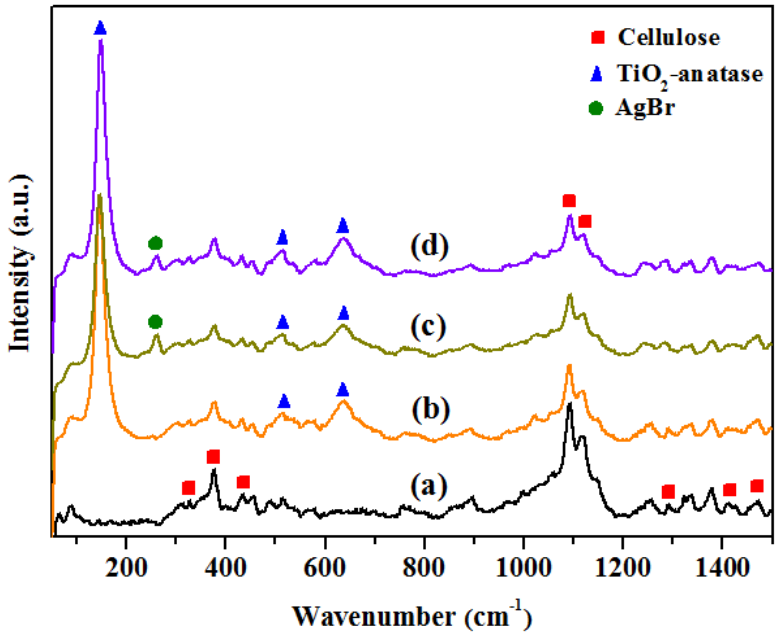

Figure 2. Raman spectra of neat paper (a), paper–TiO_2 (b), paper–TiO_2–AgBr (c) and paper–AgBr–TiO_2 (d).

After the incorporation of TiO_2 on the paper by dipping it in a pre-prepared TiO_2 solution, the bands associated with cellulose did not disappear indicating that the paper structure was maintained. Moreover, new bands at ~147, 516 and 637 cm^{-1}were observed and related to Raman-active modes of TiO_2 in anatase phase with the symmetries of E_g, $A_{1g} + B_{1g}$ and E_g, respectively (Hou et al., 2011; Ohsaka et al., 1978; Sboui et al., 2020, 2018), confirming the formation of titania on the surface of cellulose fibers.

For paper–TiO_2–AgBr and paper–AgBr–TiO_2, all the characteristic modes of the paper–TiO_2 were observed and correspond to anatase TiO_2 and cellulose I. Moreover, an additional signal was detected at 259 cm^{-1} associated with the AgBr phase (Bottger and Damsgard, 1971). The incorporation of AgBr to the catalyst for both samples, without changing the TiO_2 crystal structure, was confirmed and the order of addition of the elements during the synthesis procedure did not modify the surface crystalline species. Similar trends were confirmed by XRD and the diffractograms obtained for paper-AgBr-TiO_2 and paper-TiO_2-AgBr are presented (Fig. S1). In addition to the peaks associated with cellulose, signals related to anatase phase and AgBr were detected in both catalysts, without significant differences in the crystallinity. It is noticeable that the crystallization degree was lower than that observed for unsupported materials reported by other authors (Sui et al., 2015; Zhang et al., 2011) due to the preparation procedure over the cellulose, but it is similar between all the synthesized samples.

To better understand the morphology of the structures and the relation with the synthesis procedure, SEM images were taken and are presented in Figure 3. In the SEM images of the synthesized TiO_2 over the paper surface (Fig. 3 (A and B)), the paper fibers can be observed together with small spherical structure particles with an average diameter around 1µm that are highly dispersed onto the paper and are characteristic of TiO_2 (Ding et al., 2020).

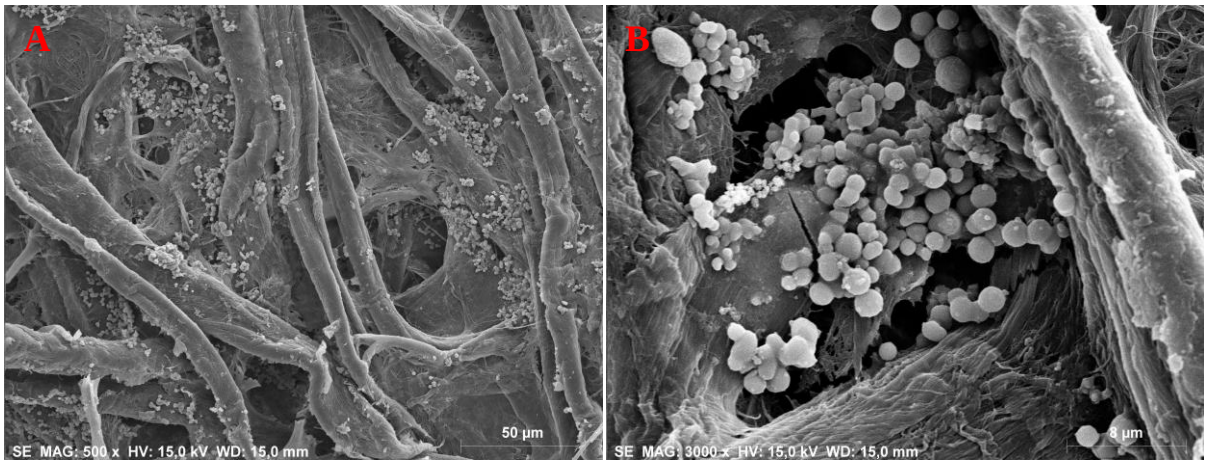

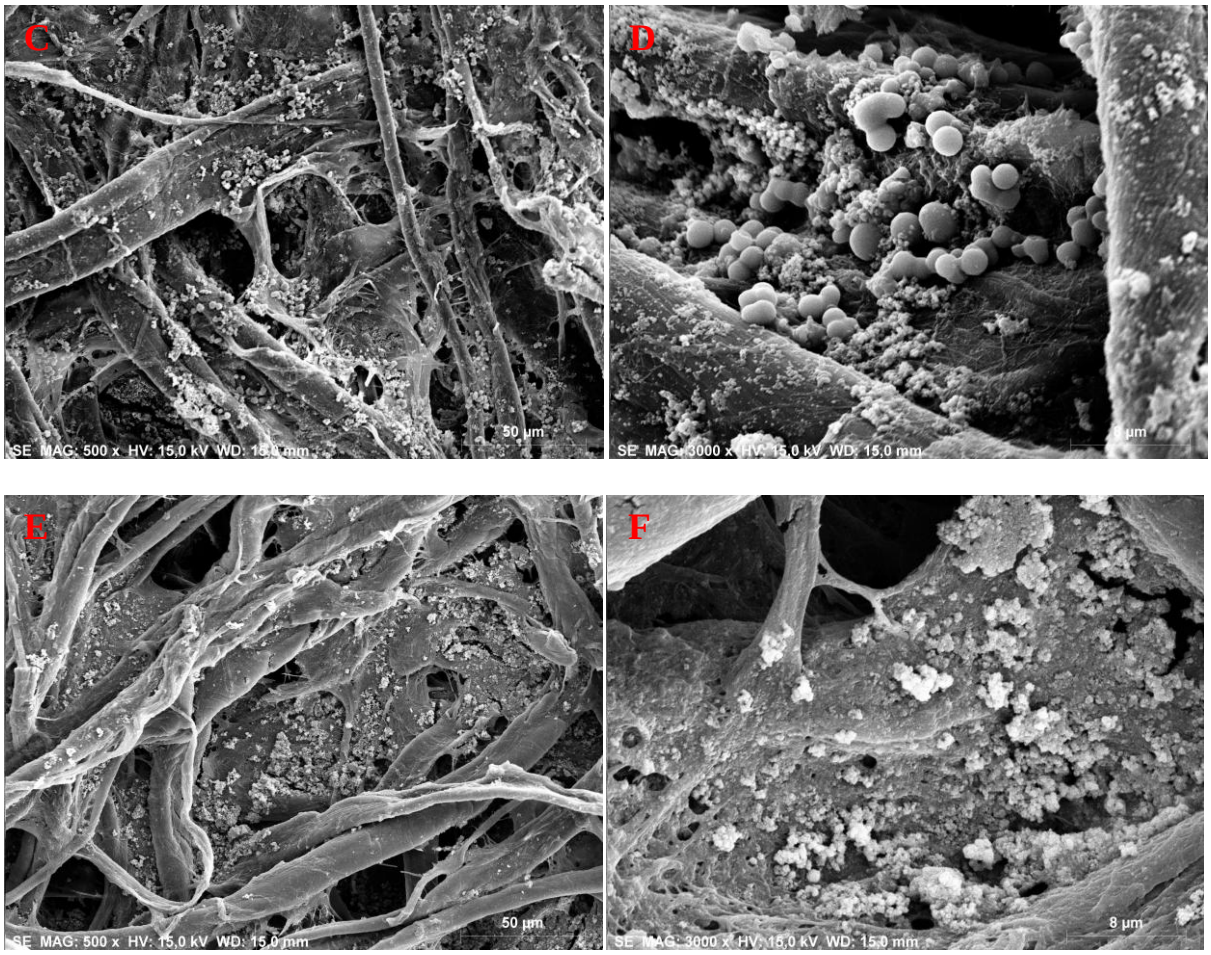

Figure 3. Images obtained by SEM of paper–TiO_2 (A, B), paper–AgBr–TiO_2 (C, D) and paper– TiO_2–AgBr (E, F).

For paper–AgBr–TiO_2 (Fig. 3 (C and D)), the images of surface showed the TiO_2 particles are dispersed on the paper fibers with similar aspect as that observed for paper–TiO_2. At higher magnification (Fig.3 D), nanoparticles dispersed on the paper fibers can be seen beside titanium oxide, which corresponds to AgBr generated before the growth of the TiO_2 nanoclusters. Therefore, the formation of AgBr and TiO_2 particles dispersed onto the paper fibers was confirmed. For paper–TiO_2–AgBr (Fig. 3 (E and F)), no noticeable change in the overall surface morphology was observed compared to paper–AgBr–TiO_2, since, in general, it is formed by paper fibers with small particles deposited in them. At higher magnification (Fig.3 F), Ag aggregate species associated with AgBr partial decomposition were homogenously

dispersed on the paper fibers, while a reduction of TiO_2 nanocluster population was observed for paper–TiO_2–AgBr.

The survey spectrum indicates the presence of Ti, Ag, O, Br and C, and Ti2p, Ag3d, O1s, Br3d and C1s regions were analyzed. XPS data of paper–AgBr–$TiO_2$and paper–TiO_2– AgBr samples are displayed in Figure 4. The titanium spectrum of both samples showed two bands centered at binding energy (BE) values of 459.3 eV and 465.2 eV, associated with $Ti2p_{3/2}$ and $Ti2p_{1/2}$ of TiO_2, respectively (Huy et al., 2019). The Ti BE values for paper–AgBr–TiO_2 and paper–TiO_2–AgBr photocatalysts were not shifted compared to those of pure TiO_2, indicating that Ag and Br species physically interact with TiO_2.

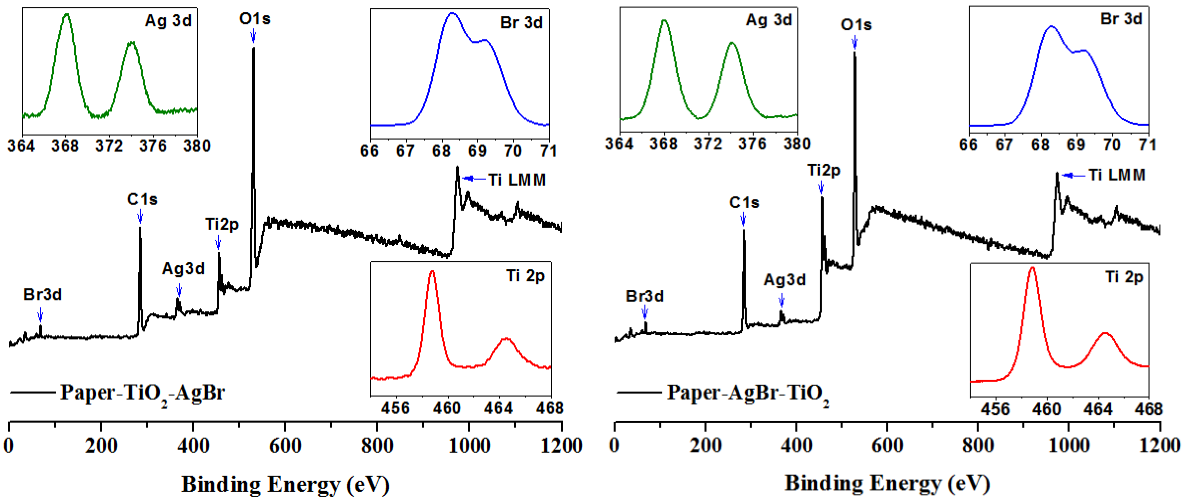

Figure 4. XPS survey of paper–TiO_2–AgBr and paper–AgBr–TiO_2. In the inset, the Ti2p, Ag3d and Br3d regions are shown.

Two peaks at 373.4 and 367.4 eV were distinguished in the Ag3d spectrum, which correspond to $Ag3d_{3/2}$ and $Ag3d_{5/2}$, respectively, of Ag^+ of the AgBr (Sui et al., 2015). Other BE for Ag were not registered and the spectrum clearly confirms the non-existence of Ag-metal species in both catalysts, which is also consistent with Raman spectra, although their presence under reaction conditions cannot be discarded. For Br3d, two specific signals localized at 68.23 eV and 69.24 eV were observed and assigned to $Br3d_{5/2}$ and $Br3d_{3/2}$, respectively, which can

be associated with Br^- in AgBr (Wang et al., 2009; Zhang et al., 2011). In addition, the C1s region was deconvoluted into three bands centered at BE values of 285.7, 286.4 and 288.0 eV. The former is attributed to the carbonyl group presence of the cellulose that acts as support and the other two weak peaks correspond to C-species contained in the cellulose paper. From XPS data, a cellulose-based hierarchical structure with TiO_2 particles decorated with a pseudo-liquid coating of Ag^+ and AgBr species can be proposed. The surface distribution depends on the incorporation order in the preparation of Ag-TiO_2 nanocomposites. As can be observed in Table 1, where the surface atomic composition registered by XPS is presented, Ag/Br and Ag/Ti atomic ratios are sensible to the formulation.

Table 1. Surface composition of the samples obtained by XPS

	O (%)	Ti (%)	Ag (%)	Br (%)
Paper–TiO_2	45.65	2.99	0	0
Paper–AgBr	34.98	0	2.64	7.93
Paper–TiO_2–AgBr	49.21	16.21	0.78	0.09
Paper–AgBr–TiO_2	46.14	3.67	0.23	0.45

The balance corresponds to carbon

The atomic ratio Ag/Br was 0.33, 0.51 and 8.67 for paper–AgBr, paper–AgBr–TiO_2 and paper–TiO_2–AgBr, respectively. Although those values are far from the stoichiometry of the Ag-precursor, apparently the incorporation of AgBr on cellulose before the addition of Ti-precursor produces a decrease in the number of silver sites that are exposed. So, the Ti/Ag atomic ratio values are close to ~ 20/1 and ~15/1 for paper–TiO_2–AgBr and paper–AgBr–TiO_2, respectively, which, additionally, presented Ag bulk content of 0.19 and 0.27 $mg \cdot g^{-1}$ by ICP measurements. These results indicated that a slight lower silver content is incorporated to the

catalyst if the surface is covered with titania, but it is more located on the surface, although in general a higher Ag/Ti ratio was found for paper-AgBr-TiO_2 material.

The SEM, Raman and XPS results show the formation of TiO_2 anatase and AgBr nanoclusters on the surface of the paper. It also gives evidence that deposition of TiO_2 and AgBr on the surface of the paper takes place for both synthesis routes, without the modification of the species, although the interaction between the species is different.

The optical properties of the photocatalysts were studied by UV–vis absorption and photoluminescence (PL) emission spectra. The UV-vis absorption spectra of neat paper, paper–TiO_2, paper–TiO_2–AgBr and paper–AgBr–TiO_2 are shown in Figure 5.

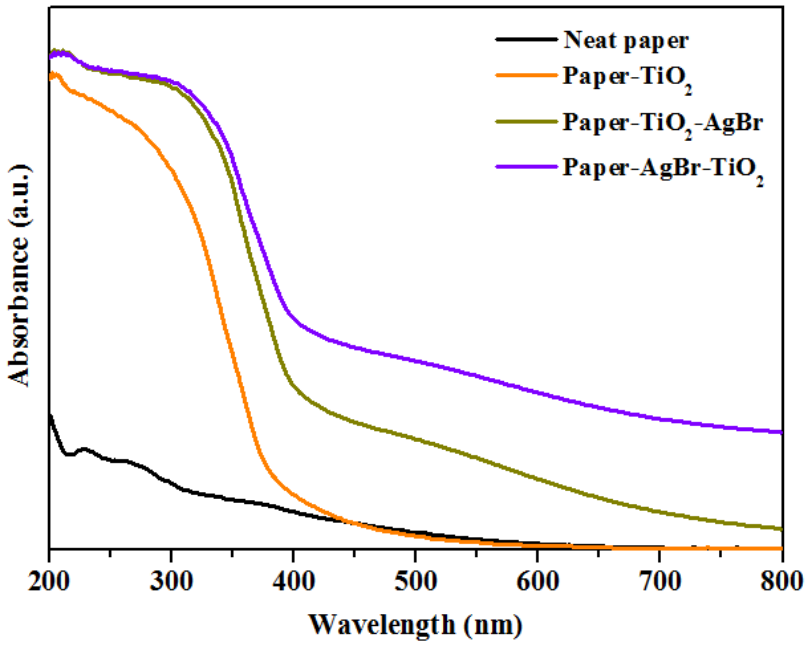

Figure 5. UV–vis spectra of neat paper (cellulose), paper–TiO_2, paper– TiO_2–AgBr and paper–AgBr–TiO_2.

As can be observed, the unmodified cellulose did not provide any absorption in the visible spectral region, with the exception of low absorption in the UV region, mainly due to side-chemical components of the cellulose. In the cellulose TiO_2-doped material a typical UV-Vis spectrum associated with TiO_2 particles, where an abrupt increase of the absorption below 400nm with a maximum at 370nm assigned to the intrinsic band-gap absorption of pure TiO_2-

anatase of ~3.2eV was registered. It was also evidenced that the incorporation of AgBr significantly affects the optical properties of TiO_2-coated cellulose and leads to the continuous absorption band in the range of 400 – 800 nm, resulting from the overlapping of Ag^+ species absorption and light absorption of silver halide (AgBr). In addition, a strong absorption in the whole UV-Vis spectra was also registered up to 800 nm (Cui et al., 2018; Wang et al., 2012). The diffuse reflectance spectra of the cellulose-based TiO_2 doped and AgBr-modified materials presented a blue-shift and increased the absorbance in the visible range depending on the order of incorporation of the photoactive components, associated with the interaction and the nature and dispersion medium composition. The blue-shift and the absorbance increment detected for paper–AgBr–TiO_2 in comparison with paper–TiO_2–AgBr should be connected with the modification of the distribution and the appearance of Ag-species, since the Ag-species population was higher for paper–AgBr–TiO_2. The extension of the absorption in Vis-region should modify the photocatalytic activity.

The photoluminescence (PL) emission of the catalysts was also measured to better understand the behavior of light-generated electrons and holes in the catalysts, because PL emission results from the recombination of free carriers. In Figure 6, the responses for paper–TiO_2, paper–TiO_2–AgBr and paper–AgBr–TiO_2 in the wavelength range from 300 to 700 nm (~4.5 – 1.5 eV) with excitation at 250nm are shown. The emission spectra profiles were similar for all the samples. A single emission signal centered at 465 nm was registered, but this broad and non-symmetrical contribution is a consequence of superimposed contributions, which should be mainly associated with direct and assisted-indirect transitions along with the contribution of other less-intense oxygen vacancies and defects related to TiO_2 (anatase) nanocrystals.

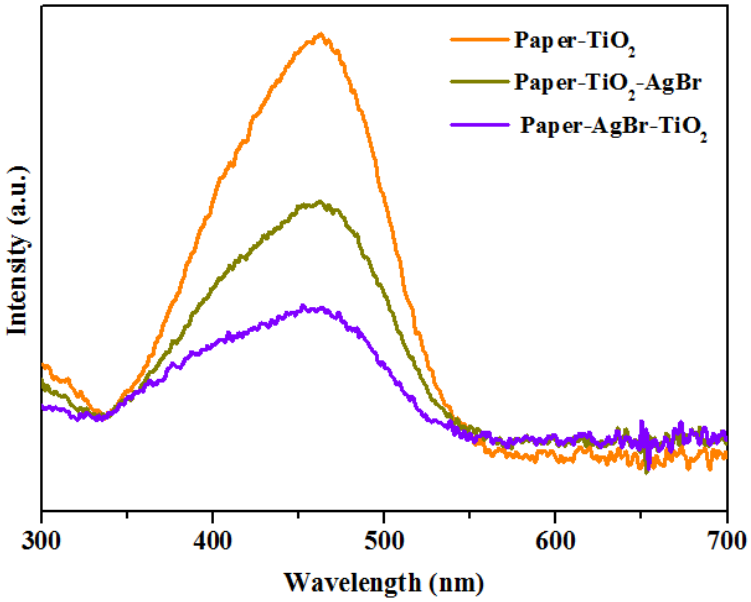

Figure 6. PL spectra of paper–TiO_2, paper–TiO_2–AgBr and paper–AgBr–TiO_2.

The PL emission spectra is further attenuated when AgBr (mainly metallic components) is incorporated to the composite. So, PL intensity for paper–AgBr–TiO_2 material is lower than that registered for paper–TiO_2–AgBr material and was attributed to the AgBr partial coverage of TiO_2 nanoclusters as was observed in SEM images. This fact suggests that a lower recombination rate of light-generated charge carriers related to charge separation efficiency was enhanced for paper–AgBr–TiO_2 catalyst, due to the Ag–Ti interaction in this material reduces the pair recombination rate of electrons and holes and increases the number of charge carriers available for photooxidation reaction promoted on TiO_2 surface.

In general, the morphology of the structures and optical properties of hybrid photocatalysts are significantly influenced by the synthesis procedures and should influence the photodegradation activity of ethanol under visible light irradiation.

3.2. Photocatalytic activity

The photocatalytic assisted aerobic-oxidation performance for the ethanol degradation, as a model of volatile organic compounds (VOCs), was analyzed over these catalysts. A series

of blank reactivity experiments of ethanol degradation was performed under the same experimental conditions, but in the absence of light or oxygen or catalyst to verify the effect of each of them on the process of degradation. All of these experiments concluded that there is no reactivity in the degradation of ethanol, which indicates that the existence of light, oxygen, and catalyst are essential elements in the process of degradation of ethanol and also the important role that all of these factors play in the photocatalytic activity. Prior the ethanol degradation process started under Xenon lamp illumination, the catalyst was placed in the reactor in dark for one hour to achieve the adsorption equilibrium. Nevertheless, it was noted that the adsorption of ethanol was permanently negligible with all prepared hybrid catalysts.

In Figure 7, the photocatalytic performance in ethanol decomposition of paper–TiO_2, paper–TiO_2–AgBr and paper–AgBr–TiO_2 is displayed, where the concentration profiles of ethanol and acetaldehyde and carbon dioxide, as intermediate products, are represented. The concentration of ethanol decreased with time whereas an increase of acetaldehyde and CO_2 was detected. It is important to note that CO_2 evolves exponentially while for acetaldehyde a maximum can be observed and coincides with the time in which ethanol concentration is almost negligible. A significant improvement in the photocatalytic performance was observed when Ag-species interact with TiO_2, since the time necessary to completely remove ethanol is reduced and the values of mineralization to CO_2 increased with a higher effect when AgBr was loaded onto the paper surface prior to TiO_2 i.e. in the case of paper–AgBr–TiO_2 compared to the photocatalytic performance of paper–TiO_2–AgBr. Although the conversion of ethanol was 100% after 5h of illumination for all catalysts, the rate of mineralization was 39.4, 61.3 and 83.4% for paper–TiO_2, paper–TiO_2–AgBr and paper–AgBr–TiO_2, respectively. So, the estimated degradation rate of ethanol increased close to 1.31 times for paper–TiO_2–AgBr and 1.72 times for paper-AgBr-TiO_2 catalysts respect to the rate registered for paper–TiO_2. This agrees that there is a synergistic effect when AgBr was incorporated onto the cellulose before

to TiO_2 as it was observed in the removal of other VOCs, such as benzene or acetone (Zhang et al., 2011). Higher conversion values than other materials containing Ag and TiO_2 used in dye removal were obtained (Bian et al., 2020; Sui et al., 2015) and also if it is compared with these species supported on natural fibers (Lopes et al., 2020), which requires 3 hours to remove anthracene in similar conditions or 2 hours at 40ºC, with a lower initial degradation rate. Although, in all cases, the incorporation of Ag to titania-based catalysts has increased the photocatalytic activity (Mkhalid et al., 2020; Sun et al., 2020), the materials presented in this work showed a higher initial ethanol removal rate, and the complete conversion of volatile compounds can be achieve in 100 minutes at room temperature, being highly active for the process.

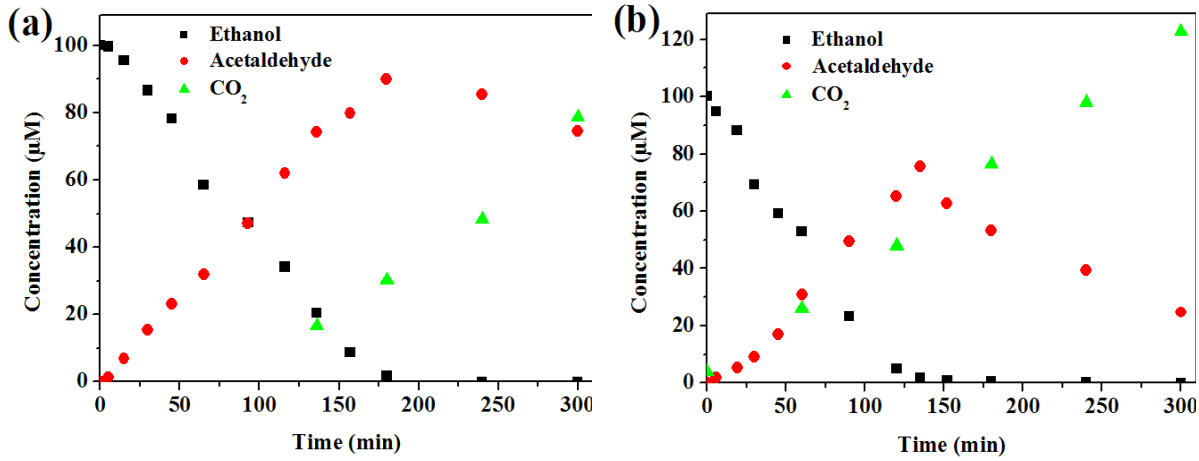

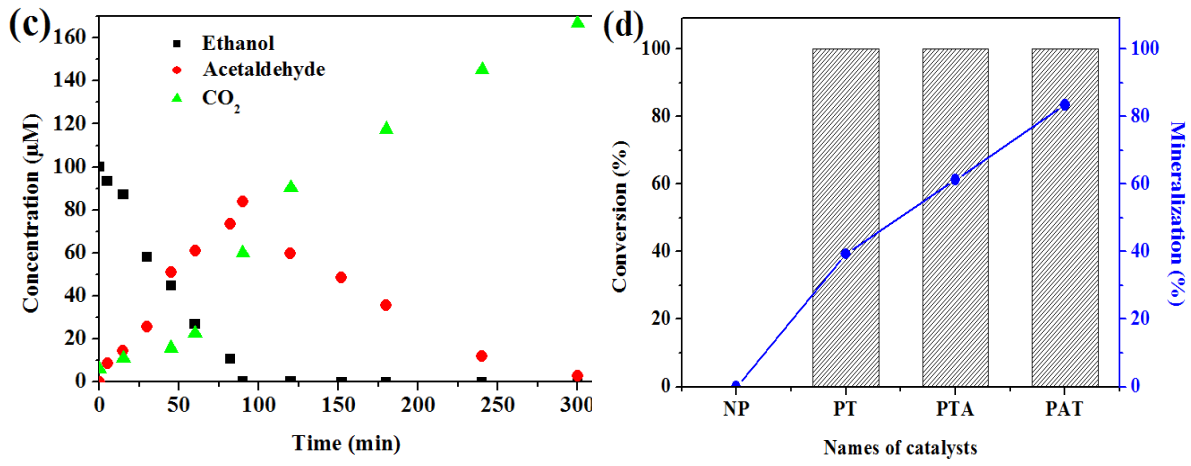

Figure 7. Photodegradation curves of ethanol and production of acetaldehyde and CO_2 versus irradiation time in the presence of paper–TiO_2 (a), paper–TiO_2–AgBr (b), paper–AgBr–TiO_2 (c) and conversion and mineralization ratio of ethanol (d). In the figure NP, PT, PTA and PAT are the abbreviations of "neat paper, paper–TiO_2, paper–TiO_2–AgBr and paper–AgBr–TiO_2", respectively.

Two routes for the mineralization of ethanol can be assumed: the direct one with CO_2 production associated with a greater consumption of ethanol and a parallel and indirect reaction that considers acetaldehyde degradation, which is favored in ethanol absence. This results from the existence of a heteroconjunction of photoactive species that favor the formation of different radical species, which are able to mineralize, and is connected with the changes in the oxidation state of carbon in ethanol (-1), acetaldehyde (+1) and CO_2 (+4) during the reaction pathway.

These results confirm the important and effective role that Ag-TiO_2 decorated species play in the ethanol photodegradation and the influence of the preparation method. The reasons for the efficiency of photodegradation of paper–AgBr–TiO_2 compared to paper–TiO_2–AgBr can be assigned to the effective interaction of TiO_2 and AgBr on paper fibers according to characterization results and the enhanced absorption in the visible domain due to the band-gap and the low recombination rate of charge carrier (Cui et al., 2018; Fu et al., 2019; Onkani et al., 2020; Wang et al., 2012).The positive effect in the catalytic performance of the band gap

406 modification and the increase of reactive oxygen species (ROS) due to the interaction of AgBr
407 and TiO_2 has been proved with a decrease in the reaction time and an increase in the
408 mineralization. Despite in both cases the same species are present, and their combination is
409 necessary to improve the activity, the order of addition of the precursors also influences the
410 performance. The incorporation of AgBr onto the surface coated with titania blocks some active
411 centers hindering the degradation routes.

412 For the AgBr–TiO_2–cellulose composite under UV light irradiation, the intensity and
413 coupling of OH–photogenerated active radicals, which come from both Ag-species and TiO_2,
414 and O_2^- radicals from Ag^+-AgBr species would be involved in the process according to
415 semiconductor combination order. An enhancement of the photocatalytic performance is
416 obtained with the use of metal coated TiO_2 nanoclusters as highly active catalysts for aerobic
417 oxidation under visible light irradiation and, consequently, paper–AgBr–TiO_2 can be
418 considered as a promising catalyst in the treatment of polluted air through its ability to
419 completely remove the pollutant. Therefore, this photocatalyst will have wide applications in
420 the improvement of air quality especially in indoor places.

421 Furthermore, the existence of an optimum concentration of AgBr for ethanol
422 photodegradation has been analyzed by changing the initial concentration of AgBr solution in
423 the synthesis of paper–AgBr–TiO_2 photocatalyst. In Figure 8 the photocatalytic performance of
424 paper–AgBr–TiO_2 prepared with different solutions of AgBr using molar concentrations from
425 $10^{-5}$to 10^{-1} M is displayed, and corresponded to Ag content in the final product of 0.005, 0.03,
426 0.27, 2.9 and 3.1 $mg \cdot g^{-1}$ according to ICP measurements. For comparison, the results for paper–
427 TiO_2 material synthesized without adding AgBr NPs are also included.

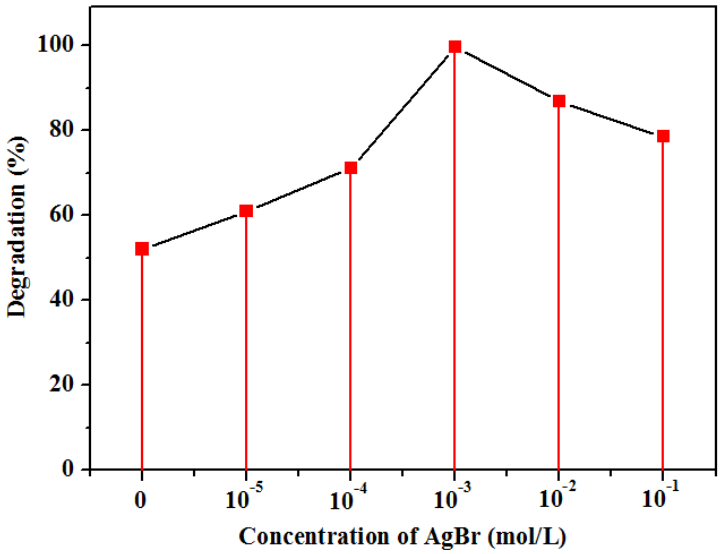

Figure 8. Effect of the concentration of the AgBr solution used to prepare paper–AgBr–TiO_2 catalysts on the photodegradation of ethanol after 90 min of irradiation.

The photocatalytic performance of paper–TiO_2 was enhanced when there is an interaction between titania and AgBr species as has been explained above. An increment of the photocatalytic performance was observed while the concentration of AgBr increased from 10^{-5} to 10^{-3}M. Nevertheless, when the concentration of AgBr solution was higher than 10^{-3} M, the degradation of ethanol started to decrease and, in consequence, the optimum concentration for AgBr is 10^{-3} M. As other authors have reported for other photocatalytic systems (Feng et al., 2015; Reddy et al., 2020), a high load of a second component over a support or several films of the same semiconductor can negatively affect to the catalytic activity, due to a reduction of the catalytic active sites. As AgBr concentration increases up to the optimum, there is an effective interaction between TiO_2 and Ag species that significantly improves the photocatalytic activity. However, if the concentration of AgBr in the synthesis solution is higher than 10^{-3} M, the amount of bulk Ag-species reaches its maximum incorporation around $3 mg \cdot g^{-1}$ and hinders the formation of the reactive oxygen species and may reduce the available charge carriers, which

445 decrease the photocatalytic performance of the paper–AgBr–TiO_2 in the degradation of ethanol
446 in gas phase.

447 Photocatalyst stability is an economical and environmental important factor, and it is
448 especially significant for photocatalysts immobilized on flexible supports such as paper.
449 Therefore, four cycles in the same experimental conditions with intermediate reactivation were
450 carried out with paper–AgBr–TiO_2 catalyst in order to verify its stability in the degradation
451 process of ethanol. The degradation percentage values obtained at the end of each cycle are
452 represented in Figure 9. Paper–AgBr–TiO_2 generally showed relatively similar degradation
453 behavior in various cycles under simulated sunlight illumination at room temperature.

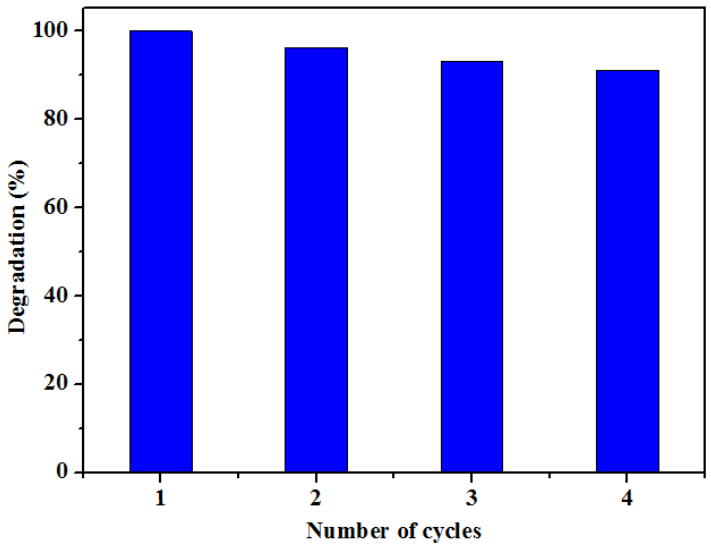

454

455 **Figure 9.** Evolution of the photodegradation efficiency of gas phase ethanol in the presence of paper–
456 AgBr–TiO_2 catalyst after four cycles of 120 min at room temperature under Xenon lamp illumination.

457

458 A remarkable 99.8% of ethanol could be degraded during the first cycle, while 91% of
459 ethanol could still be degraded by paper–AgBr–$TiO_2$for the fourth cycle, indicating the efficacy
460 and the high photocatalytic stability of paper–AgBr–TiO_2. The partial deactivation would be
461 assigned to the irreversible adsorption of partially oxidized products on the TiO_2 surface. The
462 interaction between the adsorbed species and TiO_2 leads to a decrease in the number of active

sites in the course of reaction. For the hybrid-catalyst used in this photocatalytic process, Ag^{+} species would be eventually reduced to Ag^{0} producing non-aggregated silver nanoparticles on TiO_2, as can be observed in the XRD pattern after the four cycles, where an additional peak was detected around 38.12º that is related to metallic Ag^{0} (JCPDS 04-0783), besides a slight decrease in the peaks associated with AgBr at 31 and 44.3º (JCPDS 06-0438) (Sui et al., 2015). The presence of some transitory Ag^{+} ions during the reaction should help to oxidize species adsorbed on the catalyst and regenerate and clean the surface. Therefore, the slightly deactivated paper–AgBr–TiO_2 photocatalyst is reactivated by partially oxidized products accumulated on the surface of TiO_2 that interact with Ag nanoparticles formed during the catalytic cycle.

4. Conclusions

In summary, a facile and effective strategy to incorporate AgBr/TiO_2 on paper has been proposed. A cellulose-based hierarchical structure with well dispersed TiO_2 small spherical particles around 1µm decorated with a pseudo-liquid coating of Ag^{+} and AgBr species was obtained. Paper–AgBr–TiO_2 is found to be more efficient in ethanol degradation than paper–TiO_2 and paper–TiO_2–AgBr. The incorporation of AgBr to the formulation produces the blue shift in the absorption, which increases the absorbance in the visible range. The order of addition during the synthesis influences the reactive oxygen species and the photocatalytic activity. The Ti-Ag interaction in Paper–AgBr–TiO_2 reduces the pair recombination rate and increases the available charge carriers, and, consequently, improves the photocatalytic performance of ethanol degradation. Paper–AgBr–TiO_2 was stable and reusable showing 91% efficiency even at the 4^{th} cycle.

In general, this work represents a new vision of functional materials that relies on cellulose paper as a platform, which was prepared through a simple, cost-effective and environmentally friendly method and it can be used with all flexible supports. This hybrid paper–AgBr–TiO_2 photocatalyst has several advantages: (1) the excellent ability to remove ethanol in the gas phase, which makes this hybrid material effective to treat polluted air, (2) very good stability properties with the possibility of reuse for several cycles, (3) easy to recover compared to catalysts in powder form, (4) the possibility of using sunlight as an energy source to activate the photocatalyst, which is positive in both environmental and economic terms and (5) it has wide potential for application in the environmental field and it can also be used in commercial applications as a deodorizing filter or indoor air purification.

Acknowledgements

M.S. wants to thank the financial support of Erasmus+ Project (ICM KA107).

References

Abdel Rehim, M.H., El-Samahy, M.A., Badawy, A.A., Mohram, M.E., 2016. Photocatalytic activity and antimicrobial properties of paper sheets modified with TiO_2/Sodium alginate nanocomposites. Carbohydr. Polym. 148, 194–199. https://doi.org/10.1016/j.carbpol.2016.04.061

Bian, H., Zhang, Z., Xu, X., Gao, Y., Wang, T., 2020. Photocatalytic activity of Ag/ZnO /AgO/TiO_2 composite. Phys. E Low-Dimensional Syst. Nanostructures 124, 114236. https://doi.org/10.1016/j.physe.2020.114236

Bian, Z., Tachikawa, T., Zhang, P., Fujitsuka, M., Majima, T., 2014. Au/TiO_2 superstructure-based plasmonic photocatalysts exhibiting efficient charge separation and unprecedented activity. J. Am. Chem. Soc. 136, 458–465. https://doi.org/10.1021/ja410994f

Bottger, G.L., Damsgard, C. V., 1971. Second order Raman spectra of AgCl and AgBr crystals. Solid State Commun. 9, 1277–1280. https://doi.org/10.1016/0038-1098(71)90077-9

Carbuloni, C.F., Savoia, J.E., Santos, J.S.P., Pereira, C.A.A., Marques, R.G., Ribeiro, V.A.S., Ferrari, A.M., 2020. Degradation of metformin in water by TiO_2–ZrO_2 photocatalysis. J. Environ. Manage. 262, 110347. https://doi.org/10.1016/j.jenvman.2020.110347

Chauhan, I., Aggrawal, S., Chandravati, Mohanty, P., 2015. Metal oxide nanostructures incorporated/immobilized paper matrices and their applications: a review. RSC Adv. 5, 83036–83055. https://doi.org/10.1039/c5ra13601f

Cui, Y., Zhang, Z., Li, B., Guo, R., Zhang, X., Cheng, X., Xie, M., Cheng, Q., 2018. Ultrasound assisted fabrication of AgBr/TiO_2 nano-tube arrays photoelectrode and its enhanced visible photocatalytic performance and mechanism for detoxification of 4-chlorphenol. Sep. Purif. Technol. 197, 189–196. https://doi.org/10.1016/j.seppur.2018.01.018

Daoud, W.A., Xin, J.H., 2004. Nucleation and growth of anatase crystallites on cotton fabrics at low temperatures. J. Am. Ceram. Soc. 87, 953–955. https://doi.org/10.1111/j.1551-

2916.2004.00953.x

Ding, Y., Yang, I.S., Li, Z., Xia, X., Lee, W.I., Dai, S., Bahnemann, D.W., Pan, J.H., 2020. Nanoporous TiO_2 spheres with tailored textural properties: Controllable synthesis, formation mechanism, and photochemical applications. Prog. Mater. Sci. 109, 100620. https://doi.org/10.1016/j.pmatsci.2019.100620

Feng, D., Xu, S., Liu, G., 2015. Application of immobilized TiO_2 photocatalysis to improve the inactivation of Heterosigma akashiwo in ballast water by intense pulsed light. Chemosphere 125, 102–107. https://doi.org/10.1016/j.chemosphere.2014.11.060

Ferrero, P., San-Valero, P., Gabaldón, C., Martínez-Soria, V., Penya-roja, J.M., 2018. Anaerobic degradation of glycol ether-ethanol mixtures using EGSB and hybrid reactors: Performance comparison and ether cleavage pathway. J. Environ. Manage. 213, 159–167. https://doi.org/10.1016/j.jenvman.2018.02.070

Fu, S., Yuan, W., Yan, Y., Liu, H., Shi, X., Zhao, F., Zhou, J., 2019. Highly efficient visible-light photoactivity of Z-scheme MoS_2/Ag_2CO_3 photocatalysts for organic pollutants degradation and bacterial inactivation. J. Environ. Manage. 252, 109654. https://doi.org/10.1016/j.jenvman.2019.109654

Hitam, C.N.C., Jalil, A.A., 2020. A review on exploration of Fe_2O_3 photocatalyst towards degradation of dyes and organic contaminants. J. Environ. Manage. 258, 110050. https://doi.org/10.1016/j.jenvman.2019.110050

Hou, Y., Li, X., Zhao, Q., Quan, X., Chen, G., 2011. TiO_2 nanotube/Ag-AgBr three-component nanojunction for efficient photoconversion. J. Mater. Chem. 21, 18067–18076. https://doi.org/10.1039/c1jm12788h

Huy, T.H., Phat, B.D., Kang, F., Wang, Y.F., Liu, S.H., Thi, C.M., You, S.J., Chang, G.M., Van Viet, P., 2019. SnO_2/TiO_2 nanotube heterojunction: The first investigation of NO degradation by visible light-driven photocatalysis. Chemosphere 215, 323–332.

552 https://doi.org/10.1016/j.chemosphere.2018.10.033
553 Jiménez-Tototzintle, M., Ferreira, I.J., da Silva Duque, S., Guimarães Barrocas, P.R., Saggioro,
554 E.M., 2018. Removal of contaminants of emerging concern (CECs) and antibiotic resistant
555 bacteria in urban wastewater using UVA/TiO_2/H_2O_2 photocatalysis. Chemosphere 210,
556 449–457. https://doi.org/10.1016/j.chemosphere.2018.07.036
557 Liu, S., Tang, Z.-R., Sun, Y., Colmenares, J.C., Xu, Y.-J., 2015. One-dimension-based spatially
558 ordered architectures for solar energy conversion. Chem. Soc. Rev. 44, 5053–5075.
559 https://doi.org/10.1039/c4cs00408f
560 Liu, Y., Kokot, S., Sambi, T.J., 1998. Vibrational spectroscopic investigation of Australian
561 cotton cellulose fibres. Part 1. A Fourier transform Raman study. Analyst 123, 633–636.
562 https://doi.org/10.1039/a707064k
563 Lopes, F.C.S.M.R., da Rocha, M. da G.C., Bargiela, P., Sousa Ferreira, H., Pires, C.A. de M.,
564 2020. Ag/TiO_2 photocatalyst immobilized onto modified natural fibers for
565 photodegradation of anthracene. Chem. Eng. Sci. 227, 115939.
566 https://doi.org/10.1016/j.ces.2020.115939
567 Matsubara, H., Takada, M., Koyama, S., Hashimoto, K., Fujishima, A., 1995. Photoactive TiO_2
568 containing paper: preparation and its photocatalytic activity under weak UV light
569 illumination. Chem. Lett. 767–768.
570 Mkhalid, I.A., Fierro, J.L.G., Mohamed, R.M., Alshahri, A.A., 2020. Visible light driven
571 photooxidation of imazapyr herbicide over highly efficient mesoporous Ag/Ag_2O–TiO_2 p-
572 n heterojunction photocatalysts. Ceram. Int. 1–11.
573 https://doi.org/10.1016/j.ceramint.2020.07.064
574 Ohsaka, T., Izumi, F., Fujiki, Y., 1978. Raman spectrum of anatase, TiO_2. J. Raman Spectrosc.
575 7, 321–324. https://doi.org/10.1002/jrs.1250070606
576 Onkani, S.P., Diagboya, P.N., Mtunzi, F.M., Klink, M.J., Olu-Owolabi, B.I., Pakade, V., 2020.

Comparative study of the photocatalytic degradation of 2–chlorophenol under UV irradiation using pristine and Ag-doped species of TiO_2, ZnO and ZnS photocatalysts. J. Environ. Manage. 260, 110145. https://doi.org/10.1016/j.jenvman.2020.110145

Pelton, R., Geng, X., Brook, M., 2006. Photocatalytic paper from colloidal TiO2-fact or fantasy. Adv. Colloid Interface Sci. 127, 43–53. https://doi.org/10.1016/j.cis.2006.08.002

Qian, R., Zong, H., Schneider, J., Zhou, G., Zhao, T., Li, Y., Yang, J., Bahnemann, D.W., Pan, J.H., 2019. Charge carrier trapping, recombination and transfer during TiO_2 photocatalysis: An overview. Catal. Today 335, 78–90. https://doi.org/10.1016/j.cattod.2018.10.053

Reddy, C.V., Koutavarapu, R., Reddy, K.R., Shetti, N.P., Aminabhavi, T.M., Shim, J., 2020. Z-scheme binary 1D $ZnWO_4$ nanorods decorated 2D $NiFe_2O_4$ nanoplates as photocatalysts for high efficiency photocatalytic degradation of toxic organic pollutants from wastewater. J. Environ. Manage. 268, 110677. https://doi.org/10.1016/j.jenvman.2020.110677

Sboui, M., Bouattour, S., Boufi, S., 2020. Functionalization of cotton fibers with hierarchical flower-like $Na_2Ti_3O_7$/Ag layer. Cellulose 27, 2887–2899. https://doi.org/10.1007/s10570-020-02975-4

Sboui, M., Bouattour, S., Liotta, L.F., La Parola, V., Gruttadauria, M., Marcì, G., Boufi, S., 2018. Paper-TiO_2 composite: An effective photocatalyst for 2-propanol degradation in gas phase. J. Photochem. Photobiol. A Chem. 350, 142–151. https://doi.org/10.1016/j.jphotochem.2017.09.074

Sboui, M., Nsib, M.F., Rayes, A., Swaminathan, M., Houas, A., 2017. TiO_2–PANI/Cork composite: A new floating photocatalyst for the treatment of organic pollutants under sunlight irradiation. J. Environ. Sci. 60, 3–13. https://doi.org/10.1016/j.jes.2016.11.024

Sui, Y., Su, C., Yang, X., Hu, J., Lin, X., 2015. Ag-AgBr nanoparticles loaded on TiO_2 nanofibers as an efficient heterostructured photocatalyst driven by visible light. J. Mol.

602 Catal. A Chem. 410, 226–234. https://doi.org/10.1016/j.molcata.2015.09.018
603 Sun, Y., Gao, Y., Zeng, J., Guo, J., Wang, H., 2020. Enhancing visible-light photocatalytic
604 activity of Ag-TiO_2 nanowire composites by one-step hydrothermal process. Mater. Lett.
605 279, 128506. https://doi.org/10.1016/j.matlet.2020.128506
606 Wang, P., Huang, B., Qin, X., Zhang, X., Dai, Y., Whangbo, M.-H., 2009. Ag/AgBr/$WO_3 \cdot H_2O$:
607 Visible-light photocatalyst for bacteria destruction. Inorg. Chem. 48, 10697–10702.
608 https://doi.org/10.1021/ic9014652
609 Wang, S.-H., Wang, K.-H., Dai, Y.-M., Jehng, J.-M., 2013. Water effect on the surface
610 morphology of TiO_2 thin film modified by polyethylene glycol. Appl. Surf. Sci. 264, 470–
611 475. https://doi.org/10.1016/j.apsusc.2012.10.046
612 Wang, W.-S., Du, H., Wang, R.-X., Wen, T., Xu, A.-W., 2013. Heterostructured
613 Ag_3PO_4/AgBr/Ag plasmonic photocatalyst with enhanced photocatalytic activity and
614 stability under visible light. Nanoscale 5, 3315–3321. https://doi.org/10.1039/c3nr00191a
615 Wang, W., Jing, L., Qu, Y., Luan, Y., Fu, H., Xiao, Y., 2012. Facile fabrication of efficient
616 AgBr-TiO_2 nanoheterostructured photocatalyst for degrading pollutants and its
617 photogenerated charge transfer mechanism. J. Hazard. Mater. 243, 169–178.
618 https://doi.org/10.1016/j.jhazmat.2012.10.017
619 Xu, J., Dai, G., Chen, B., He, D., Situ, Y., Huang, H., 2020. Construction of Ti^{3+}-TiO_2-C_3N_4por
620 compound coupling photocatalysis and Fenton-like process: Self-driven Fenton-like
621 process without extra H_2O_2 addition. Chemosphere 241, 125022.
622 https://doi.org/10.1016/j.chemosphere.2019.125022
623 Zhang, N., Yang, M.-Q., Liu, S., Sun, Y., Xu, Y.-J., 2015. Waltzing with the versatile platform
624 of graphene to synthesize composite photocatalysts. Chem. Rev. 115, 10307–10377.
625 https://doi.org/10.1021/acs.chemrev.5b00267
626 Zhang, Y., Tang, Z.-R., Fu, X., Xu, Y.-J., 2011. Nanocomposite of Ag-AgBr-TiO_2 as a

627 photoactive and durable catalyst for degradation of volatile organic compounds in the gas
628 phase. Appl. Catal. B Environ. 106, 445–452.
629 https://doi.org/10.1016/j.apcatb.2011.06.002
630
631